Int J Adv Struct Eng (2016) 8:53–71
DOI 10.1007/s40091-016-0114-0

ORIGINAL RESEARCH

Seismic response of an elevated aqueduct considering hydrodynamic and soil-structure interactions

Bhavana Valeti[1] · Samit Ray-Chaudhuri[1] · Prishati Raychowdhury[1]

Received: 1 March 2015 / Accepted: 4 February 2016 / Published online: 25 February 2016

Abstract In conventional design of an elevated aqueduct, apart from considering the weight of water inside the channels, hydrodynamic forces are generally neglected. In a few special cases involving high seismic zones, hydrodynamic forces have been modeled considering equivalent lumped-mass type idealization or other models. For support conditions, either the base is considered as fixed or in a few cases, equivalent spring-dashpot system is considered. However, during an intense seismic event, nonlinear soil-structure interactions (SSI) may alter the response of the aqueduct significantly. This paper investigates the effect of hydrodynamic forces and SSI on seismic response of a representative elevated aqueduct model. Different modeling concepts of SSI has been adopted and the responses are compared. Frequency domain stochastic response analysis as well as time-history analysis with a series of ground motions of varying hazard levels have been performed. Demand parameters such as base shear and drift ratio are studied for varying heights of water in channels and different site conditions. From the frequency domain analysis, the effect of convective masses is found to be significant. From the time history analysis, the overall effect of increase in height of water is found to be negligible for nonlinear base case unlike the fixed and elastic base cases. For the nonlinear base condition, the base shear demand is found to decrease and the drift ratio is found to increase when compared to the results of linear base condition. The results of this study provide a better understanding of seismic behavior of an elevated aqueduct under various modeling assumptions and input excitations.

✉ Prishati Raychowdhury
prishati@iitk.ac.in

[1] Indian Institute of Technology Kanpur, Kanpur, India

Keywords Elevated aqueduct · Seismic response · Hydrodynamic effects · Soil-structure interaction · Stochastic response · Nonlinear time-history analysis

Introduction

Aqueducts are man made structures that have been crucial part of every civilization in the distribution of the essential but not so ubiquitous element of nature, water. Aqueducts transport water across topographical barriers to their destination, taking various forms and traveling at different levels with respect to the ground such as pipelines and canals. An elevated aqueduct is a bridge that crosses barriers such as a valley or a river, often accommodating road and water transport systems.

The massive load of water in an elevated aqueduct shifts its center of mass further above the ground compared to highway/railway bridges. As a result, the structure becomes more vulnerable to dynamic lateral forces, especially, those due to hydrodynamic effects. In addition, for estimation of seismic response, a fixed base assumption for stiff structures such as an aqueduct, may often lead to an inappropriate design if the soil underneath is not so stiff. Consideration of nonlinear SSI in such a situation can yield a more realistic appraisal of the behavior of soil-foundation interface during strong earthquakes. This is because the nonlinear SSI can take into account the energy dissipation behavior and nonlinear variation of stiffness along the soil-foundation interface.

(a) *Hydrodynamic forces* A water bearing structure experiences hydrodynamic forces when subjected to inertial forces. Such dynamic forces were first taken into account by Westergaard (1933) for determining the dynamic pressures due to water on a rectangular

dam with a vertical face. Perhaps Housner (1954) was the first to propose a method to model dynamic effects of fluid in accelerated containers in terms of convective and impulsive pressures. Liu (1981) applied a Lagrangian-Eulerian method for the kinematical description of fluid-structure interaction. Ramaswamy and Kawahara (1987) analyzed large free surface motions in the fluid domain including sloshing using an arbitrary Lagrangian-Eulerian kinematical description. A particle finite element method was used by Idelsohn et al. (2006) to discretize the fluid continuum into particles. A number of studies were carried out on the hydrodynamic effects of ground supported water tanks. Details of these studies can be found in Valeti (2013).

(b) *SSI effects* In current practice, although nonlinear design of superstructure is accepted to meet its ductility demand, the foundations are generally designed to remain in linear zone. This is because of the difficulty in inspection and repair of highly deformed foundations along with the concern in reliable estimation of nonlinear soil-foundation responses. Gutierrez and Chopra (1978) evaluated the methods for seismic analysis of SSI, namely, simple general substructure methods and direct finite element method. Impedance functions for horizontal and coupled degrees of freedom were developed for soil modeled as both uniform viscous medium and layered soil over uniform viscous medium (Wong and Luco 1985; Gazetas 1991b). Harden et al. (2005) calibrated the model parameters for the Beam-on-nonlinear-winkler-foundation (BNWF) model. This model was subsequently updated by Raychowdhury and Hutchinson (2009) and a command *ShallowFoundationGen* was introduced in the OpenSees (2012) platform. Raychowdhury (2011) and Raychowdhury and Singh (2012) studied the effects of soil compliance and nonlinearity in low-rise steel moment-resisting frames subjected to earthquake ground motions of varying hazard levels. It is clear from the aforementioned discussions that SSI and hydrodynamic forces may be crucial for performance assessment of elevated aqueducts under significant earthquake loading. However, as per authors' knowledge, not much work has been done so far considering these aspects. The present study addresses these two important issues to develop a better understanding of seismic behavior of an elevated aqueduct under various modeling assumptions and input excitations. For this purpose, a simplified model of an elevated aqueduct is considered. Different base fixity conditions such as fixed-base, elastic-base and nonlinear base conditions are considered. Housner's model is used to represent water in aqueduct channels for seismic analysis. For nonlinear SSI model, the 'Beam-on-Nonlinear-Winkler-Foundation (BNWF)' concept is used. Time history analyses are performed with a series of ground motions of varying hazard levels to study the effect of nonlinear SSI. Demand parameters such as base shear and drift ratio are studied for varying heights of water in channels and different soil conditions at the site.

Numerical modeling

Seismic analysis of an elevated aqueduct involves developing appropriate models to represent: (1) structural model of the aqueduct, (2) hydrodynamic effects between water and aqueduct, and (3) SSI effects between soil and foundation. The following subsections provide a detailed discussion of the numerical modeling approach for the aforementioned components:

The superstructure of an elevated aqueduct comprises the deck slab and walls, which in turn rest on substructure, i.e., on piers and abutments. Bearings are used between the deck and substructure to restrict any vertical or transverse relative movement of the deck. Only limited movement is allowed in the longitudinal direction to accommodate thermal expansions. The deck conveys water through a single or multiple channels separated by walls. The foundations underneath the pier walls can either be deep or shallow depending soil conditions. In addition to the loads acting on a typical (railway/highway) bridge, forces due sloshing and impact of water inside the channels act laterally. This makes an aqueduct more vulnerable to seismic forces compared to (railway/highway) bridges.

In this study, Arjun Feeder Canal Aqueduct proposed to be constructed across Birma river located in the state of Madhya Pradesh (India) is representatively modeled. The aqueduct considered is 188.4 m long from abutment to abutment with 13 spans each 14.5 m long. The deck is 31.5 m wide with a slab of thickness 0.65 m and is equally divided into four channels, each of width (L) 6.938 m. The channels are separated by 3.11 m high walls of 0.75 m thickness each. The deck is at an average height of (H_a) 15 m. The pier walls are 34.5 m long (L_p) and 1.732 m thick (B_p). The foundation is a raft connecting all the pier walls between the abutments (see Fig. 1).

For simplicity of modeling, only a representative portion of the aqueduct is modeled as a single-degree of freedom (SDOF) system. For this purpose, a tributary span of the deck on a single pier is idealized as a classically damped, linear, SDOF system with mass m_p concentrated at an

effective height H_p as shown in Fig. 1. The mass m_p comprises of (1) mass of deck, (2) impulsive mass of water and (3) mass from top half portion of the pier wall. The stiffness of the superstructure (K_p) is calculated from the stiffness of the pier. The pier wall is numerically modeled using *ElasticBeamColumnElement* in OpenSees (2012). A damping ratio of 5 % is used for modeling of the aqueduct structure.

In Fig. 1, also shown are the convective water masses connected with representative springs. In this study, Housner's model (Housner 1954) (see Fig. 2) is employed in the calculation and modeling of the dynamic pressure distribution in terms of convective and impulsive masses acting on the walls of a channel of the aqueduct. For unit length of the aqueduct, the equivalent impulsive mass M_o due to static pressure distribution in a channel is represented as mass rigidly attached to the walls at a height H_o. Housner (1954) defined impulsive mass according to Eqs. (1) and (2). Here, H is the height of water in the aqueduct channel, L is half of the width of the channel and M is the mass of water per unit length of the channel.

$$H_o = \frac{3}{8}H \tag{1}$$

$$M_o = M\frac{\tanh(\sqrt{3}L/H)}{\sqrt{3}L/H} \tag{2}$$

For unit length of the aqueduct, the sloshing effect of water in channel is represented by an equivalent convective water mass M_n (Housner 1954). This mass is assumed to be attached to the walls at a height H_n with stiffness K_n as given in Eqs. (3)–(5).

$$M_n = M\frac{1}{3}\sqrt{\frac{5}{2}\frac{L}{H}}\tanh\left(\sqrt{\frac{5}{2}\frac{H}{L}}\right) \tag{3}$$

$$H_n = H\left[1 - \frac{1}{\sqrt{\frac{5}{2}\frac{H}{L}}\tanh\sqrt{\frac{5}{2}\frac{H}{L}}} + \frac{1}{\sqrt{\frac{5}{2}\frac{H}{L}}\sinh\sqrt{\frac{5}{2}\frac{H}{L}}}\right] \tag{4}$$

$$K_n = \left(\omega_n^2\right)M_n = \frac{3gHM_n^2}{L^2M} \tag{5}$$

For modeling of the hydrodynamic effects, separate impulsive and convective masses are computed for each channel of the aqueduct for unit length. These masses are then computed for the tributary length of the aqueduct channels. The walls of the aqueduct are assumed to be rigid and the static pressure acting on the bottom of the aqueduct channels are neglected. Figure 3 shows modeling of impulsive and sloshing masses for the aqueduct channels. Here, in each channel, m_o represents the impulsive mass, m_{si} is the convective mass and k_{si} is the total stiffness of springs connecting the convective mass with the channel structure. These impulsive masses are then added to the mass of the aqueduct while equivalent convective masses are fixed on top of the structure with a uniaxial springs in the transverse direction of the aqueduct (see Fig. 1). Housner's parameters for different heights of water in each channel of the aqueduct for a unit length are as shown in Table 1 for increasing heights of water up to 3 m. In addition to these, a damper with damping ratio of 0.1 % is

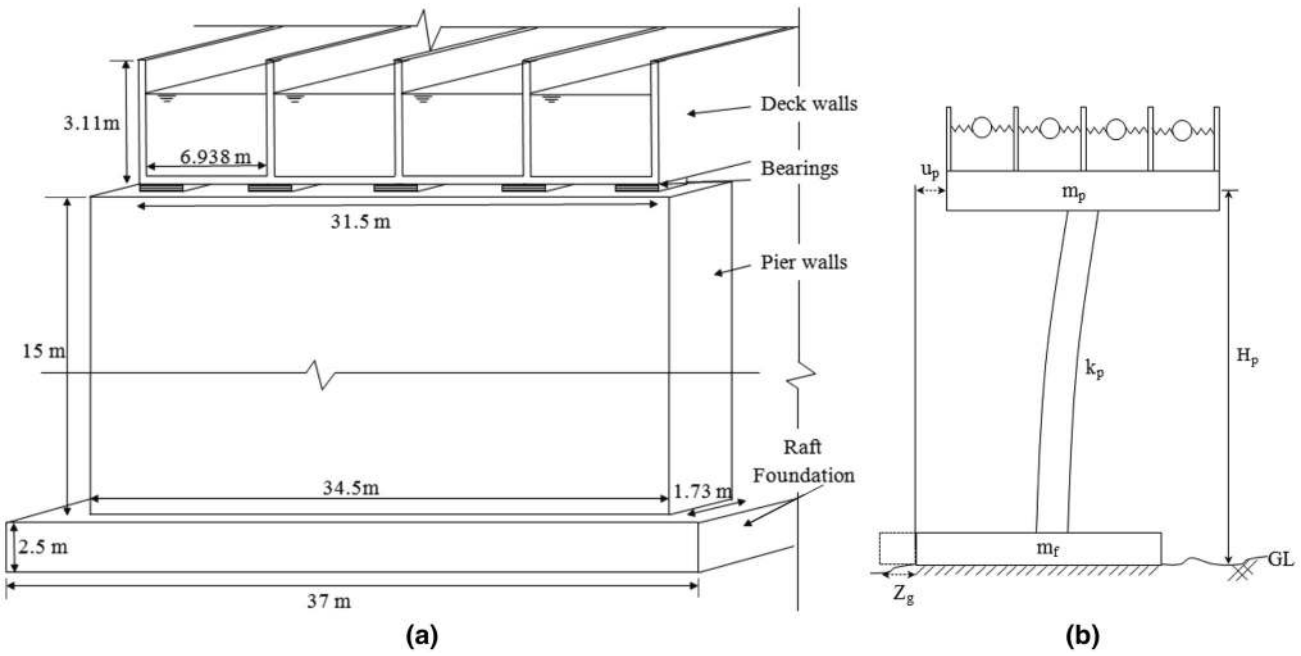

Fig. 1 **a** Schematic diagram of aqueduct in transverse direction and **b** lumped mass model for fixed-base aqueduct

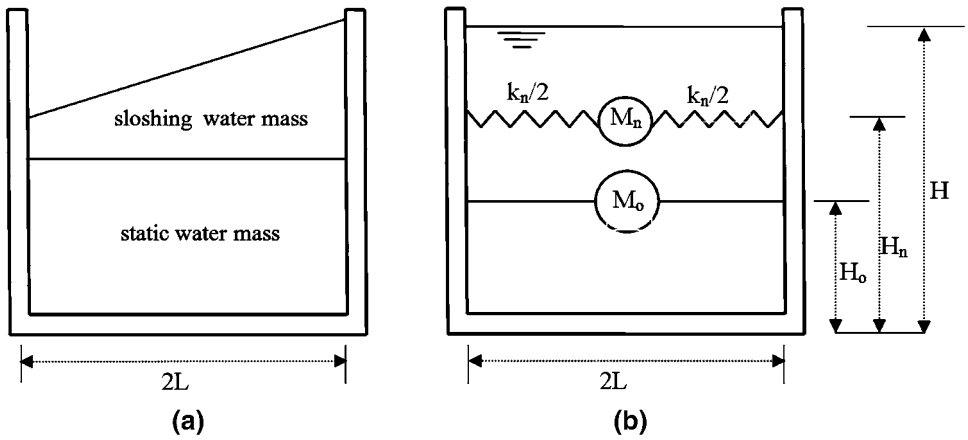

Fig. 2 **a** Sloshing and impulsive masses of water and **b** Housner's model representation

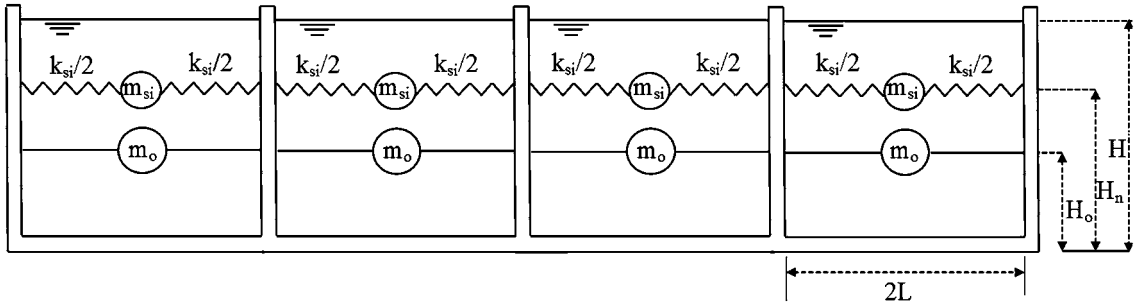

Fig. 3 Housner's representation of hydrodynamic effects in aqueduct channels

Table 1 Parameters for Housner's model

H (m)	M (kg)	M_o (kg)	m_{si} (kg)	k_{si} (kN/m)	H_o (m)	H_1 (m)	ω_{si} (rad/s)
0.5	25,150.25	20,603.09	20,638.30	2092.89	0.19	0.25	1.00
1.0	50,300.5	39,236.89	74,851.16	8371.48	0.38	0.51	1.38
1.5	75,450.75	54,619.35	145,044.89	18,823.56	0.56	0.78	1.63
2.0	100,601	66,389.10	214,290.49	33,322.11	0.75	1.06	1.80
2.5	125,751.3	74,881.88	272,623.22	51,473.93	0.94	1.37	1.90
3.0	150,901.5	80,754.25	317,059.08	72,648.91	1.13	1.70	1.98

added with each sloshing mass to provide additional energy dissipating mechanism during sloshing.

Modeling of SSI

The foundation for the representative portion of the structure is assumed as a shallow foundation with 14.5 m along the longitudinal direction of aqueduct (i.e, along the deck) and 34.5 m in the transverse direction (across the deck) and 1.5 m deep. The foundation is assumed to be a mat foundation resting on the ground. For the shake comparison of responses, the soil-foundation interface is modeled as fixed, elastic and nonlinear base cases.

Modeling of linear SSI for frequency domain analysis Gazetas (1991a) impedance functions are employed to model SSI in frequency domain analysis. The foundation is assumed to be rigid, massless and placed on a homogeneous elastic half-space, which replicates a reasonably deep, uniform soil deposit (Gazetas 1991a). Since, impedance functions are dependent on soil properties, geometry of foundation and excitation frequency, they are suitable in the stochastic response analysis considering SSI in frequency domain. The impedance function (S) for a given degree of freedom can be written as:

$$S = \tilde{K} + i\omega C \tag{6}$$

where ω is excitation frequency

$$\tilde{K} = Kk(\omega) \tag{7}$$

$$i\omega C = \left(C_{rad} + \frac{2\tilde{K}}{\omega}\beta\right) \tag{8}$$

Here, K is the static stiffness for a given footing and soil parameters; $k(\omega)$ is the dynamic stiffness coefficient dependent on excitation frequency and acquired from experimental results for different foundation geometries and soil properties (Gazetas 1991b). The complex damping component $i\omega C$ is a combination of radiation damping C_{rad} and inherent material damping $\frac{2\tilde{K}}{\omega}\beta$, which are dependent on excitation frequency, and β is the material damping constant of the soil. The soil parameters that have been used for different soil conditions for the calculation of impedance functions are as given in Table 2.

Modeling of SSI for time-history analysis Modeling nonlinear SSI for shallow foundations requires a model to capture the nonlinear soil-foundation behavior such as, temporary gap formation, foundation settlement, sliding and hysteretic energy dissipation. BNWF (Harden et al 2005) is one such model implemented in OpenSees (2012) with the aforementioned attributes. In BNWF model elastic foundation is modeled with discrete finite elements defined using ElasticBeamColumnElements (OpenSees 2012). Compound nonlinear independent zero-length winkler springs are attached to these foundation elements. These are defined by nonlinear hysteretic materials (QzSimple, PySimple, TzSimple materials Boulanger et al. 1999). These nonlinear springs are a combination of dashpots, and drag and gap elements that define the soil-foundation interaction by capturing horizontal ($p -x$), vertical ($p -z$), shear-sliding ($t -x$) and moment rotation behaviors at the base of the footing. The *ShallowFoundationGen* (Raychowdhury and Hutchinson 2008) command is used to model the soil-foundation interface with lesser inputs from the user reducing the manual task of defining each element of the soil-foundation system. It uses the concept of BNWF. The command also provides options for the degree of flexibility at the soil-foundation interface as shown in Fig. 4, where k_{in} represent the initial stiffness of of foundation springs. Input parameters for foundation modeling in OpenSees using *ShallowFoundationGen* are as discussed here. The soil properties of the clayey soils considered are taken as in Table 2. The dimensions of foundation are 37 m long, 6 m wide, and 2.5 m deep. A nominal embedment depth of 0.01 m is considered for the convenience of analysis. For mesh generation, *ShallowFoundationGen* requires the input for the following factors: (a) stiffness intensity ratio (R_k) for vertical springs at the end of the footing to those at the middle, which is taken as 2, (b) end length ratio (R_e) between length of the stiffened ends to the length of the foundation, which is taken as 0.2, and (c) vertical spacing (S_e) between the springs as fraction of total footing length, which is taken as 0.2.

Table 2 Soil parameters (Bowles 1988)

Soil type	Poison′sratio (v)	Shear wave velocity (V_s, m/s)	Density (ρ, kg/m^3)	Elastic modulus (E_s, 10^6 N/m^2)	Cohesion (c, N/m^2)
Soft	0.2	100	1750	25	25,000
Medium	0.325	200	1950	50	75,000
Firm	0.4	300	2250	100	150,000

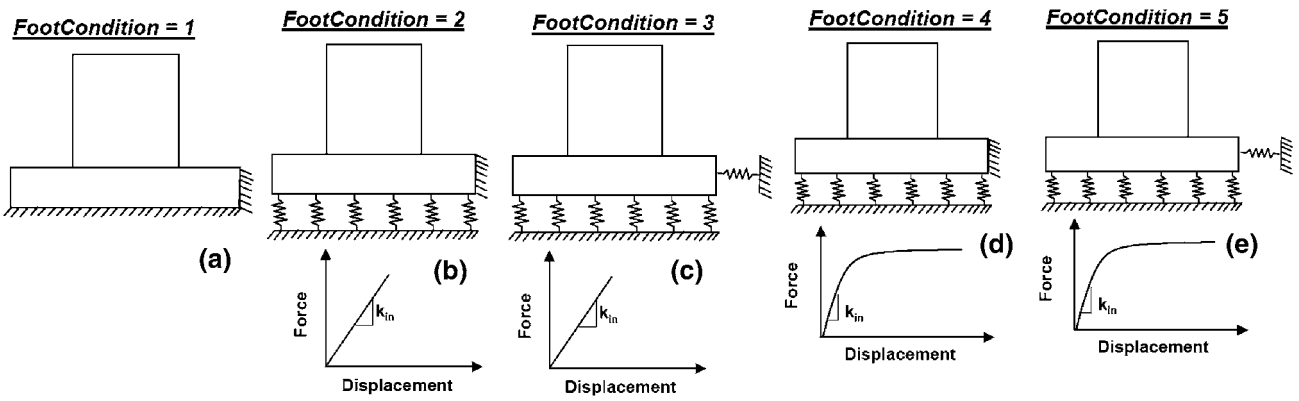

Fig. 4 Different footing conditions: **a** fixed base, **b** elastic base with no sliding allowed, **c** elastic base with sliding allowed, **d** nonlinear base with no sliding and **e** nonlinear base with sliding unrestricted (Raychowdhury and Hutchinson 2008)

Eigenvalue analysis

Eigenvalue analyses are performed for the model aqueduct for different heights of water including only the impulsive water masses. The foundation is modeled using *ShallowFoundationGen* command (OpenSees 2012) with different base fixity conditions. The natural periods for the fixed-base aqueduct structure (i.e., along the transverse direction of the aqueduct channels) are found to be very low. The increase in the periods is observed with the augmentation of flexibility due to soil at the base. For zero water height the period of the structure increased from 0.025 s for the fixed-base case to 0.52, 0.59, and 0.743 s for firm, medium and soft soil conditions, respectively. The periods have increased more than ten times with the flexibility at the base. This drastic increase in period from the fixed to flexible base case can be explained by considering the relative stiffness of the structure in comparison to the foundation springs. The stiffness of the representative model in this direction is very high due to a very long shear wall (34.5 m long and 1.732 m thick) and hence, the fixed base period is found to be very low. However, when the flexible base condition is considered, the rocking mode (due to foundation springs) influences the fundamental period significantly, even for the firm base condition. And hence, the period increases significantly even for the firm base condition. This is because, the stiffness of the foundation due to springs (even in case of firm condition) is much lower than that of the structure. To study the effect of varying water level in channels, the normalized fundamental periods of the structure for different height of water in the channels (and for the fixed and different elastic base conditions) are shown in Fig. 5. The normalization has been done with respect to the period when the aqueduct is empty. Hence, all the curves for different base conditions start from unity. The variation of impulsive masses with height is not significant enough to notably change the period of the highly stiff aqueduct structure. A shoot up of periods of structure is not linear for any soil condition, as the increase in the impulsive mass is nonlinear and also the masses added are so small compared to the structural mass that this addition cannot lead to a linear increase in the periods.

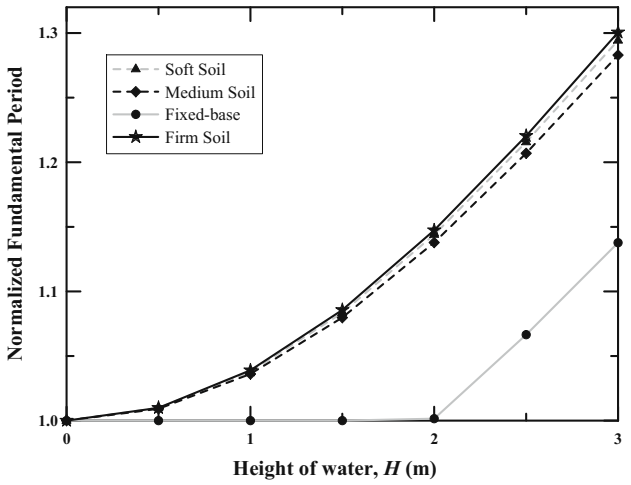

Fig. 5 Comparison of normalized natural periods of structure for different base conditions and for varying height of water

Seismic analysis of aqueduct

This section describes the analysis procedures for the frequency domain and time-history analysis of the elevated aqueduct model considered in this study.

Frequency domain analysis

In frequency domain analysis, fixed-base and elastic base conditions for the foundation model are considered. The details of these analyses are provided as follows:

Fixed-base case Consider a linear, classically damped fixed-base SDOF structure with mass m_p, stiffness k_p and damping c_p. Let u_p denote the displacement at the top of the fixed-base structure relative to the base. Let m_{si} be the ith convective water mass attached to the aqueduct structure through springs of total stiffness k_{si} and damping coefficient c_{si}, where $i = 1, 2, \ldots, n$. Let u_{si} be the displacement of ith convective mass with respect to its base (see Fig. 6). The equations of motion for the structure and the convective water masses subjected to free-field horizontal ground acceleration, $\ddot{Z}_g(t)$ (in the transverse direction of aqueduct) can be written as follows:

For aqueduct structure,

$$m_p\ddot{u}_p(t) + c_p\dot{u}_p(t) + k_p u_p(t) - \sum_{i=1}^{n} k_{si}u_{si}(t) - \sum_{i=1}^{n} c_{si}\dot{u}_{si}(t) = -m_p\ddot{Z}_g(t) \tag{9}$$

For water masses,

$$m_{si}\ddot{u}_{si}(t) + c_{si}\dot{u}_{si}(t) + k_{si}u_{si}(t) = -m_{si}\ddot{Z}_g(t) - m_{si}\ddot{u}_p(t), \quad i = 1, 2, \ldots, n \tag{10}$$

Taking Fourier transform and on further simplifications, the displacement response of the aqueduct structure in frequency domain can be written as follows:

$$u_p(\omega) = \frac{H_f(\omega)\left(-1 + \frac{1}{m_p}\sum_{i=1}^{n} v_i(\omega)h_{si}(\omega)\right)}{1 + \frac{H_f(\omega)}{m_p}\omega^2 \sum_{i=1}^{n} v_i(\omega)h_{si}(\omega)}\ddot{Z}_g(\omega) \tag{11}$$

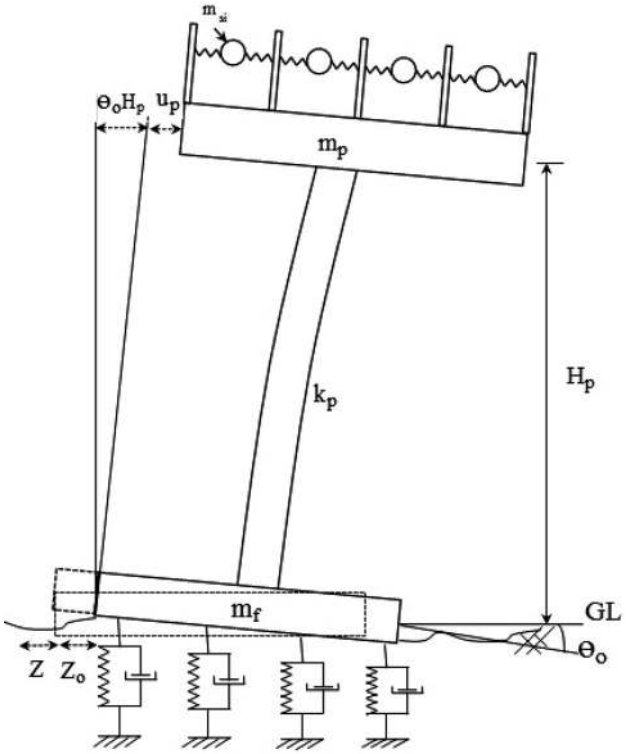

Fig. 6 Lumped mass representative model for flexible-base case

where ω_p is the fixed-base natural frequency and ζ_p is the damping ratio of the aqueduct structure; ω_{si} (with $i = 1, 2, \ldots, n$) are the natural frequencies and ζ_{si} are the damping ratios of water masses; $H_f(\omega)$ is the transfer function of fixed-base aqueduct structure and $h_{si}(\omega)$ (with $i = 1, 2, \ldots, n$) are the transfer functions of fixed-base equivalent convective water masses.

The coefficient of $\ddot{Z}_g(\omega)$ in Eq. (11) is the transfer function say $T_F(\omega)$, for the displacement of fixed-base aqueduct structure $u_p(\omega)$ and horizontal ground acceleration at the base $\ddot{Z}_g(\omega)$.

$$T_F(\omega) = \frac{H_f(\omega)\left(-1 + \frac{1}{m_p}\sum_{i=1}^{n} v_i(\omega) h_{si}(\omega)\right)}{1 + \frac{H_f(\omega)}{m_p}\omega^2 \sum_{i=1}^{n} v_i(\omega) h_{si}(\omega)} \tag{12}$$

Multiplying each side of Eq. (11) with respective complex conjugates, can be written as the spectral density function (PSDF),

$$u_{\mathrm{pPSD}}(\omega) = |T_F(\omega)|^2 \ddot{Z}_{gPSD}(\omega) \tag{13}$$

The root mean square response $u_{prms}(\omega)$ for the displacement of the aqueduct structure can be calculated as

$$u_{\mathrm{prms}}(\omega) = \sqrt{\sum_{i=1}^{N} |T_F(\omega)|^2 \ddot{Z}_{gPSD}(\omega)\Delta\omega} \tag{14}$$

where $\Delta\omega$ is the appropriate frequency interval and $\omega = \omega_{\max}/N$ with N being number of intervals.

Elastic-base case In the flexible-base case (see Fig. 6), when subjected to ground acceleration $\ddot{Z}_g(t)$, the aqueduct experiences forces due to interaction accelerations, $\ddot{Z}_o(t)$ and $\ddot{\theta}_o(t)$, inertial force due to its own mass $m_p\ddot{u}_p(t)$, and forces transferred from the water masses $c_{si}\dot{u}_{si}(t) + k_{si}u_{si}(t)$ (with $i = 1, 2, \ldots, n$). Note that the free-field rocking is neglected. The system equations are as follows for the aqueduct structure and the convective water masses, can be written as follows:

$$\begin{aligned} &m_p\ddot{u}_p(t) + c_p\dot{u}_p(t) + k_p u_p(t) - \sum_{i=1}^{n} k_{si}u_{si}(t) - \sum_{i=1}^{n} c_{si}\dot{u}_{si}(t) \\ &\quad = -m_p\left(\ddot{Z}_g(t) + \ddot{Z}_o(t) + H_p\ddot{\theta}_o(t)\right) \end{aligned} \tag{15}$$

$$\begin{aligned} &m_{si}\ddot{u}_{si}(t) + c_{si}\dot{u}_{si}(t) + k_{si}u_{si}(t) \\ &\quad = -m_{si}\left(\ddot{Z}_g(t) + \ddot{Z}_o(t) + H_p\ddot{\theta}_o(t)\right) - m_{si}\ddot{u}_p(t), \\ &\quad i = 1, 2, \ldots, n \end{aligned} \tag{16}$$

Taking Fourier transform for Eqs. (15) and (16) and on further simplifications, acceleration response $\ddot{u}_p(\omega)$ obtained as follows (see details in Valeti 2013):

$$\begin{aligned} \ddot{u}_p(\omega) = \omega^2 H_f(\omega)\Big(&\ddot{Z}_g(\omega) + \ddot{Z}_o(\omega) + H_p\ddot{\theta}_o(\omega) \\ &- \frac{1}{m_p}\sum_{i=1}^{n} v_i(\omega)u_{si}(\omega)\Big) \end{aligned} \tag{17}$$

where $u_p(\omega)$, $u_{si}(\omega)$, $\ddot{Z}_g(\omega)$, $\ddot{\theta}_o(\omega)$ and $\ddot{Z}_o(\omega)$ denote Fourier transforms of $u_p(t)$, $u_{si}(t)$, $\ddot{Z}_g(t)$, $\ddot{\theta}_o(t)$ and $\ddot{Z}_o(\omega)$ respectively. Relationships of foundation accelerations $\ddot{Z}_o(\omega)$, $\ddot{\theta}_o(\omega)$ with hydrodynamic forces $\sum_{i=1}^{n}(k_{si} + i\omega c_{si})u_{si}(\omega)$ and ground acceleration $\ddot{Z}_g(\omega)$ are established using impedance functions, base shear and base moment equations of the aqueduct structure. According to Dey and Gupta (1999), if the foundation is assumed to be massless, then base shear $V_s(\omega)$ and base moment $M_s(\omega)$ can be expressed in terms of foundation displacements relative to the soil medium using the impedance functions.

$$\begin{Bmatrix} V_s(\omega) \\ \dfrac{M_s(\omega)}{L} \end{Bmatrix} = \begin{bmatrix} S_{xx} & S_{x-ry} \\ S_{ry-x} & S_{ry} \end{bmatrix} \begin{Bmatrix} Z_o(\omega) \\ L\theta_o(\omega) \end{Bmatrix} \tag{18}$$

Here S_{xx}, S_{ry}, S_{x-ry} and S_{ry-x} are the impedance functions for translation in transverse direction, rotation about the longitudinal direction and coupled translation and rotation of the foundation respectively. As the foundation is assumed to be resting on the surface of the ground, moment due to the reaction from soil on to the side walls of the

foundation is neglected. As a result, the coupled impedance functions S_{x-ry} and S_{ry-x} are almost negligible.

Using expressions for base shear and base moment from Eq. (18) in the base shear and base moment equations and substituting $\ddot{u_p}(\omega)$ from Eq. (17) and replacing $Z_o(\omega)$, $\theta_o(\omega)$ by $\frac{\ddot{Z}_o(\omega)}{-\omega^2}$, $\frac{\ddot{\theta}_o(\omega)}{-\omega^2}$ respectively, we obtain equations which contain the terms of only ground translation ($\ddot{Z}_g(\omega)$), relative translational ($\ddot{Z}_o(\omega)$) and rotational $\ddot{\theta}_o(\omega)$ accelerations of foundation with respect to soil and aqueduct-water masses interaction forces.

Solving the resulting simultaneous equations, one can obtain expressions for $\ddot{Z}_o(\omega)$ and $\ddot{\theta_o}(\omega)$ as follows, where Q_1, P_1 represent transfer functions between input free-field ground acceleration $\ddot{Z}_g(\omega)$ and interaction accelerations $\ddot{Z}_o(\omega)$, $\ddot{\theta_o}(\omega)$ respectively. Similarly Q_2, P_2 are the transfer functions between aqueduct-water masses interaction forces $\sum_{i=1}^{n} v_i(\omega)u_{si}(\omega)$ and interaction accelerations $\ddot{Z}_o(\omega)$, $\ddot{\theta_o}(\omega)$ respectively (Ray Chaudhuri and Gupta 2003).

Now, the forces transferred by fixed-base water masses to aqueduct structure, $\sum_{i=1}^{n} v_i(\omega)u_{si}(\omega)$, the transfer function $TF(\omega)$ between relative displacement of aqueduct structure $u_p(\omega)$ and ground acceleration $\ddot{Z}(\omega)$ is obtained as

$$\mathrm{TF}(\omega) = \frac{H_f(\omega)\left(-\left(1+Q_1+H_pP_1\right)+\frac{\sum_{i=1}^{n} v_i(\omega)h_{si}(\omega)\left(\frac{-1}{m_p}+Q_2+H_pP_2\right)\left(1+Q_1+H_pP_1\right)}{1+\left(Q_2+H_pP_2\right)\sum_{i=1}^{n} v_i(\omega)h_{si}(\omega)}\right)}{1+H_f(\omega)\frac{\sum_{i=1}^{n} v_i(\omega)h_{si}(\omega)\left(\frac{-1}{m_p}+Q_2+H_pP_2\right)}{1+\left(Q_2+H_pP_2\right)\sum_{i=1}^{n} v_i(\omega)h_{si}(\omega)}} \tag{19}$$

Time-history analysis

For time-history analysis, the raft foundation resting on the surface of soil, is modeled using *ShallowFoundationGen* command in the framework of OpenSees (2012). To capture the behavior under varying soil conditions, soft, medium and firm states of clayey soils are considered for the analysis. In addition, to study the effect of different base conditions, the foundation is modeled for fixed, linear and nonlinear degrees of flexibility. A vertical factor of safety of $FS_v = 5$ is used for modeling of the foundation.

Transient ground motion analyses are performed for different heights of water for the fixed, linear, and nonlinear base conditions. A gravity analysis is performed and the response results are hold. After that the transient analyses are performed. These transient analyses are performed using *Newmark*'s integration with $\gamma = 0.5$, $\beta = 0.25$. Unlike frequency domain, damping due to the water is neglected and Rayleigh damping is assumed for the structure. For analysis, *NewtonLineSearch* algorithm is used with a limiting ratio 0.8 and a tolerance of 10^{-18} in the framework of OpenSees (2012).

Results and discussion

The results of the frequency domain and time-history analyses are presented and the observations are discussed as follows.

Frequency domain results

Clough-Penzien power spectral density functions (PSDF) (Villaverde 2009) have been used to represent the input free-field accelerations for soft, medium and firm soil conditions. The parameters for these PSDFs (as given in Table 3) are obtained from Kiureghian and Neuenhofer (1992) except for the medium soil condition for which an interpolation technique is used. The resulting Clough-Penzien PSDFs for all three soil types are shown in Fig. 7. One can observe from this figure that a reduction in amplitude, an increase in spread and a shift towards higher frequencies with an increase in stiffness of the soil.

Fixed-base case Displacement transfer functions relating u_p with ground acceleration for different heights of

Table 3 Clough-Penzien parameters (Kiureghian and Neuenhofer 1992)

Soil type	G_o	ω_g (rad/s)	ω_1 (rad/s)	ζ_g	ζ_1
Soft	0.05	5.0	0.5	0.2	0.6
Medium	0.05	10.0	1.0	0.4	0.6
Firm	0.05	15.0	1.5	0.6	0.6

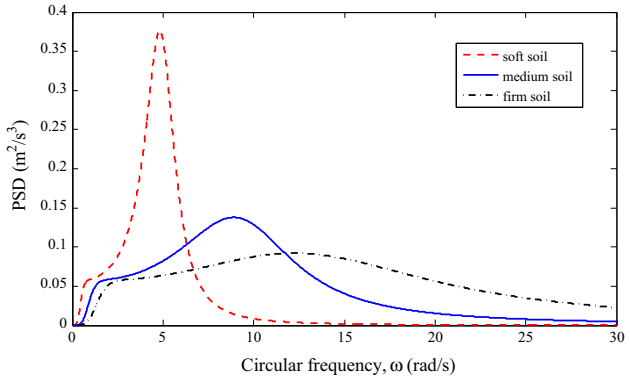

Fig. 7 Clough-Penzien PSDFs for different soil types

water (H) are obtained as shown in Fig. 8. Here, for a given height of water, the first peak from the origin corresponds to the vibration mode of the aqueduct structure whereas the other peaks (on right) represent the sloshing modes. It may be noted that all the sloshing modes (one mode for each of the four channels) are appearing approximately in the same period location. This is because the mass representing the sloshing modes of each channel are equal. A nominal shift towards right corresponding to the first peak (structure) is observed with increasing height of water due to the addition of impulsive water masses. Further, a significant shift towards left is observed for the sloshing modes, indicating its increasing frequency along with the height of water.

Clough-Penzien PSDFs of different soil site conditions are used as the free-field input acceleration PSDFs to obtain the PSDFs of responses of the structure. Figure 9 show the power spectral density (PSD) of u_p with different site conditions. From Fig. 9a–c, the influence of the input PSDFs on u_p can be clearly observed, with a visible peak at period 1.256 s observed in case of soft soil site (at the dominant frequency of the input soft soil site PSDF). Similar peaks are observed at 0.628 s and 0.418 s, respectively, for PSDFs corresponding to medium and firm soil sites. The magnitude of these peaks reduces with an increase in stiffness of the underlying soil. A similar trend is also observed for base shear PSDFs and not shown here to save space.

RMS values of u_p, base shear, and drift ratio for different heights of water in the aqueduct and different soil sites are obtained. Figure 10 shows the normalized RMS values for the base shear, V_b. Here, the normalization is done with respect to the maximum base shear, i.e., V_b corresponding to the water height $H = 3$ m for firm site. It is observed from this figure that RMS values of displacement for different heights of water do not follow a linear trend. In fact, a small peak is observed for the mid height of water. However, the maximum base shear occurs at full water height. This phenomenon can be explained by looking at the trend of amplitude of peaks at fixed-base natural periods of convective water masses in the transfer function in conjunction with Clough-Penzien PSDF (see Fig. 7). Hence, one can say that the RMS values of displacement are dominated by the response of the convective water masses. A similar trend is also observed for the RMS values of base shear and percentage drift ratio.

Elastic-base case Transfer functions $T_F(\omega)$ and PSDFs are obtained for u_p, base shear, V_b, and drift ratio in all three soil site conditions conditions. Figures 11 and 12 respectively show $T_F(\omega)$ and PSDFs of u_p for different soil site conditions. By comparing Fig. 8 with Fig. 11, one can notice that the peak corresponding to the structure period is almost insignificant in the elastic-base case. This can be clearly observed in Figs. 11d and 12d which, respectively, compare the transfer functions and PSDFs of fixed and elastic base cases (firm soil) for at 1.5 m height of water. This is because of period elongation combined with higher damping due to SSI. But, no such effect of base flexibility is observed on sloshing modes. The significant separation between the structure mode and sloshing modes (sloshing modes are highly flexible compared to the structure mode), changes the structural responses but cannot significantly affect the sloshing mode responses.

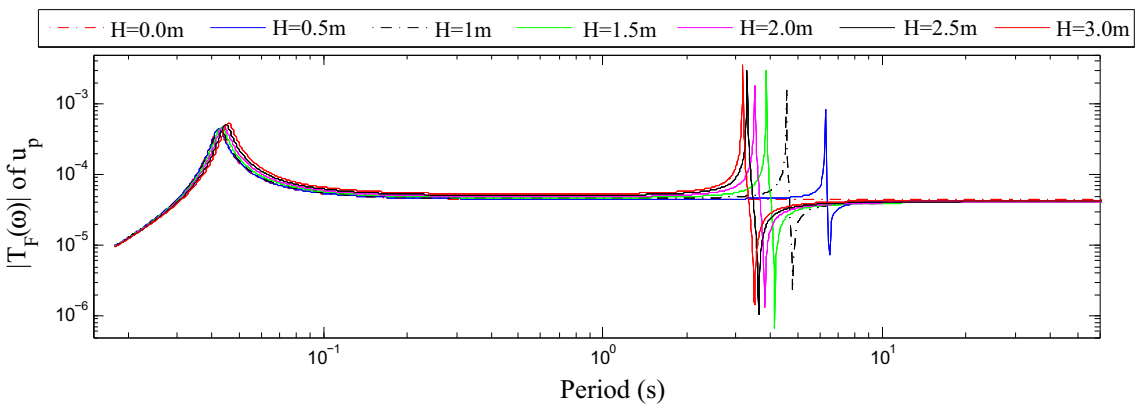

Fig. 8 Transfer functions for u_p evaluated using fixed-base analysis

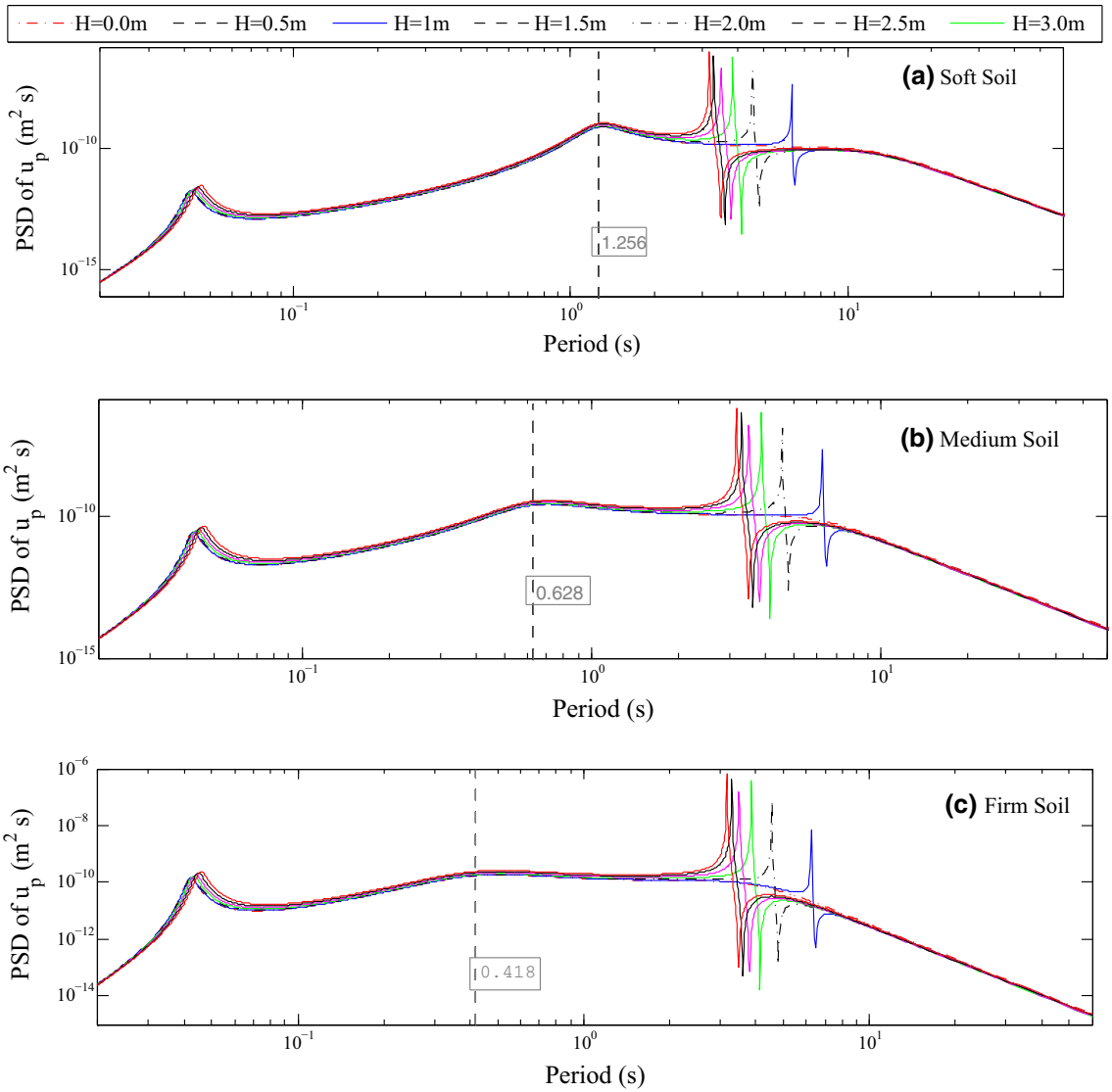

Fig. 9 PSDF of u_p evaluated using fixed-base analysis with underlying soil as: **a** soft, **b** medium and **c** firm

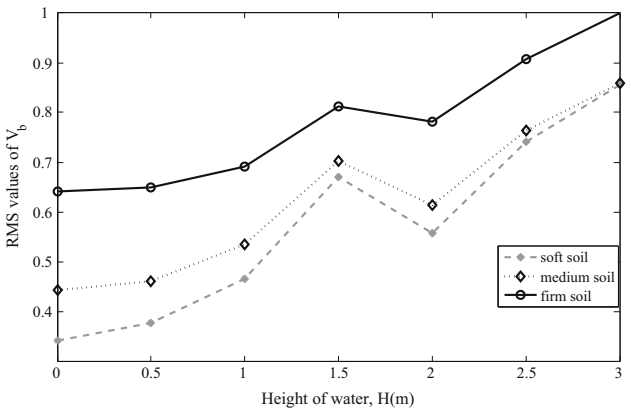

Fig. 10 Normalized RMS values of base shear, V_b evaluated using fixed-base analysis

RMS values for displacement of aqueduct structure (u_p) are calculated from the PSDFs obtained earlier and are normalized for different heights of water and soil conditions. Similarly, the RMS values for the base shear and percentage drift ratio are also obtained. Figure 13 provides the RMS values of V_b with varying water height for different soil site conditions. It is evident that the response of the structure follows the same trend as that of the magnitude of convective water masses of different heights for all soil conditions, as in fixed-base case the input PSDFs have invariant magnitudes for different soil conditions at the natural period of the structure. Also, the base shear increases with an increase in height of water due impulsive masses of water, being highest at the full water level.

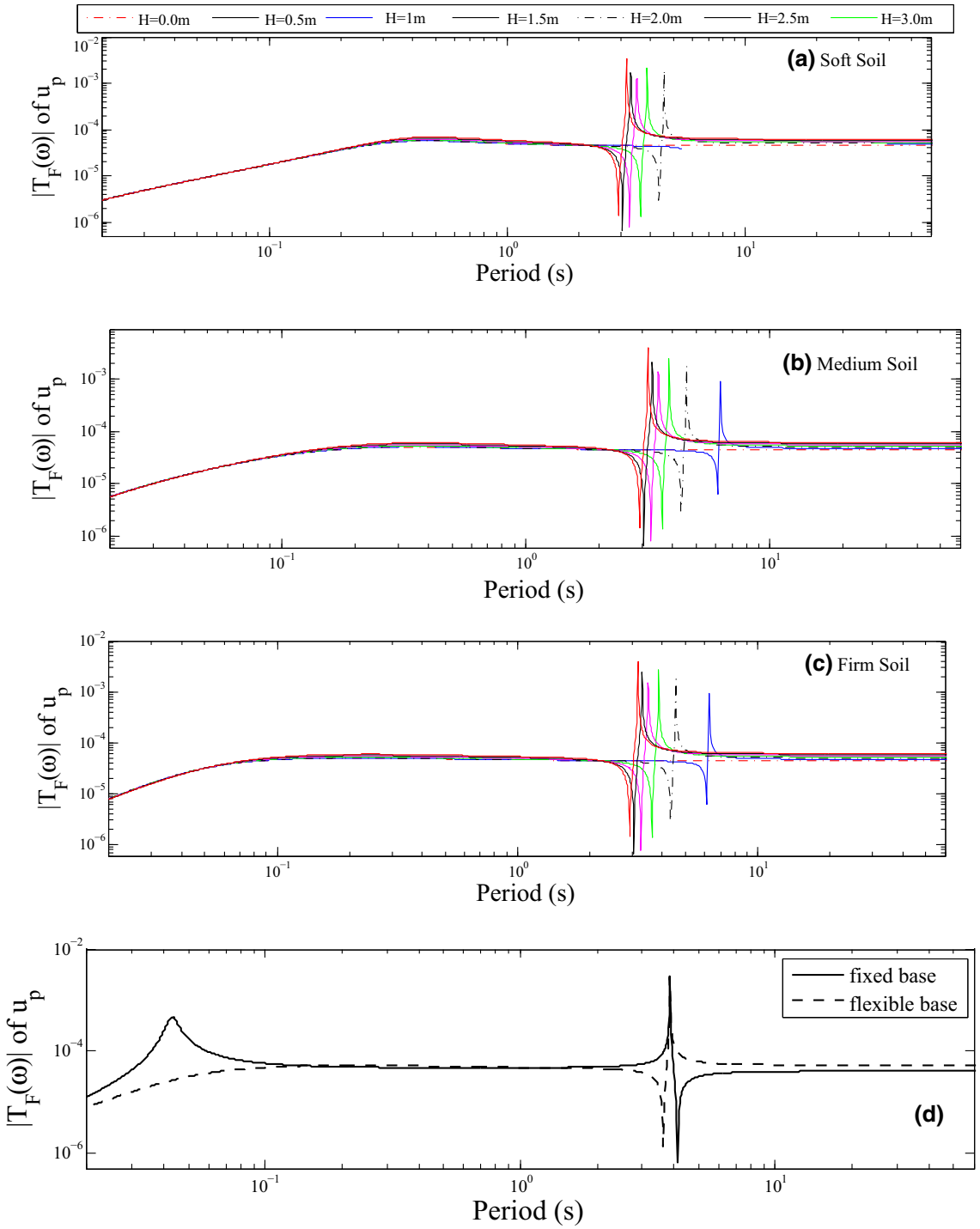

Fig. 11 Transfer functions of u_p (evaluated using flexible-base analysis) for soil conditions: **a** soft, **b** medium, **c** firm and **d** comparison of transfer functions of u_p for water height of 1.5 m and firm soil site (evaluated using fixed base and flexible-base analyses)

Time-history analysis

Sixty records of horizontal acceleration time histories that were generated for the Los Angeles region under FEMA/SAC steel building project (http://www.sacsteel.org/project/) are used as input ground excitations. There are 30 pairs of ground motions with each pair consisting of a fault parallel and a fault normal component of a single ground motion. Out of 30 pairs, there are 10 pairs for each of 3 different hazard levels namely, probability of exceedence of 2 % in 50 years (LA21–LA40), 10 % in 50 years (LA01–LA20) and 50 % in 50 years (LA41–LA60).

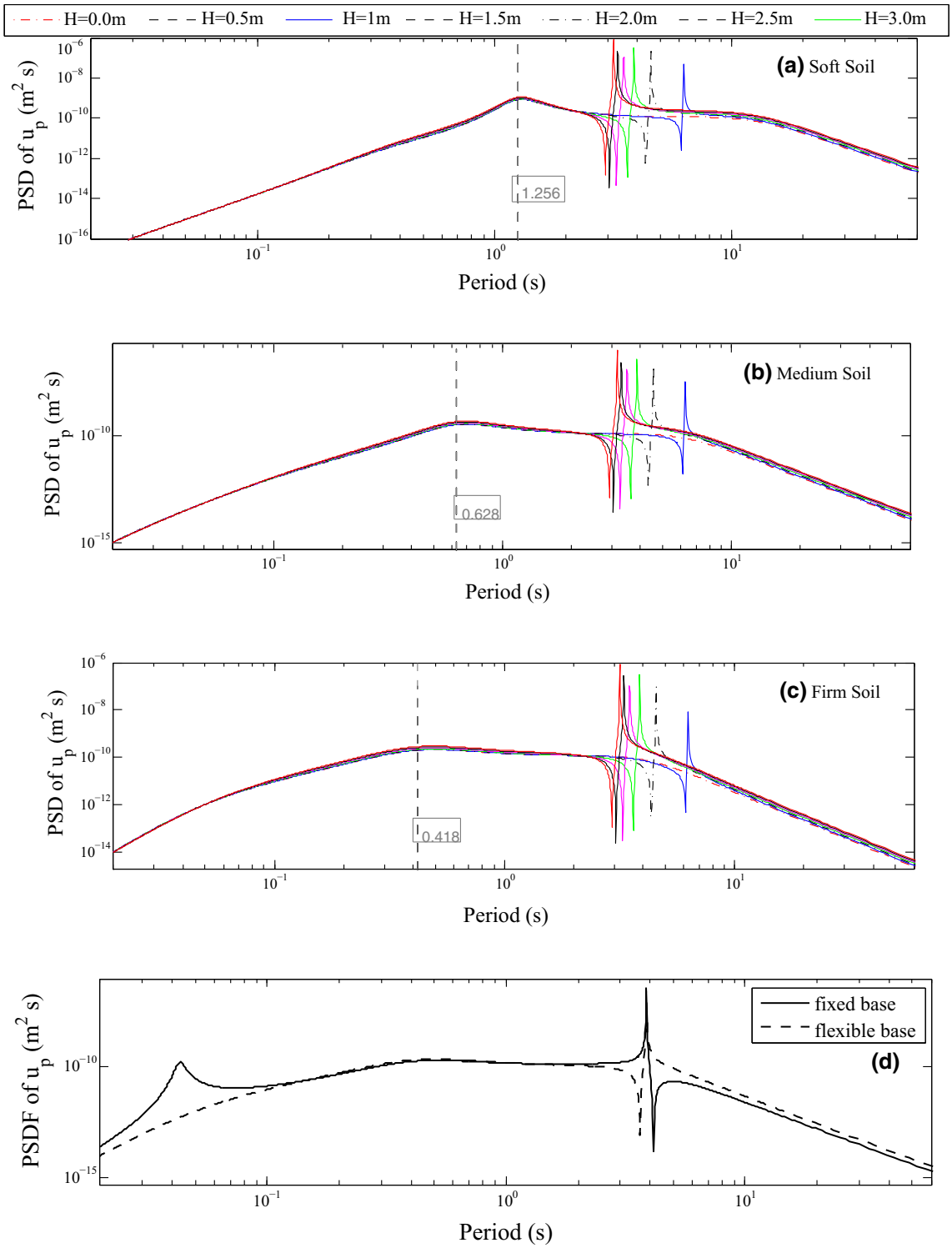

Fig. 12 PSDFs of u_p (evaluated using flexible base analysis) for soil conditions: **a** soft, **b** medium, **c** firm and **d** comparison of PSDFs of u_p for water height of 1.5 m and firm soil site (evaluated using fixed base and flexible-base analyses)

At first, a gravity analysis is performed and then holding the states, time history analysis is performed. Response parameters such as base shear (recorded as the reaction at the base node of the structure) and drift ratio (i.e., relative displacement between the nodes at base and top of the structure normalized by the height) are recorded for comparison. The mean and standard deviation for the peak base shear and peak drift ratio for different heights of water and

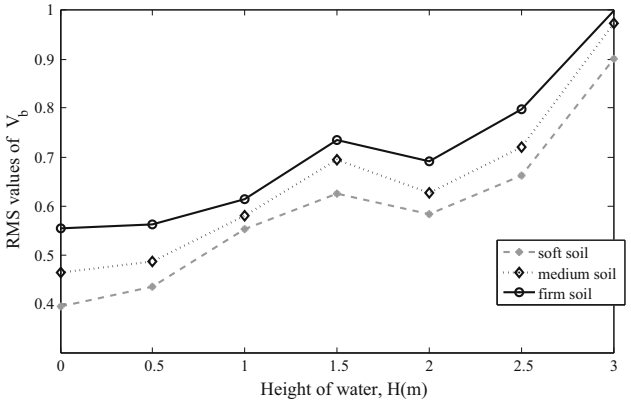

Fig. 13 Normalized RMS values of base shear, V_b (evaluated using flexible-base analysis) for different soil conditions

for each of the three hazard levels of ground motions are evaluated.

Fixed-base case ShallowFoundationGen command with *FootingCondition* 1 is used for the fixed-base case (fixed in all degrees of freedom). The mean (μ) and coefficient of variation (c_v) values of the peak base shear for different heights of water under all three hazard levels of ground motions are shown in Fig. 14. It is found from Fig. 14 that the mean peak base shear values increase with an increase in the height of water and the hazard level of the ground motions. With height of water, the increase in mean values does not follow a linear trend. The local peak at 1.5 m of water (that was earlier observed for the RMS values) is not observed here. This is because the SAC ground motions do not have sufficient energy content to meaningfully excite a sloshing mode. The peak drift ratios (percentage values) also follow the same trend. The c_v values do not show any trend with water height. One can notice that as the hazard level increases, mean response increases and c_v reduces.

Linear elastic-base case For the time-history analysis of elastic-base case, the *FootingCondition* 3 is used. Gazetas (1991b) static (linear) stiffness values are used at the soil-foundation interface for different degrees of freedom that is sliding, vertical and rotation (Raychowdhury and Hutchinson 2008).

Mean values of peak base shear and drift ratio for different soil conditions and heights of water for different hazard levels are obtained (Fig. 15). In general, for hazard levels of 10 % in 50 years and 50 % in 50 years, the force demands are highest for the firm soil and lowest for soft soils. However, this is not clearly observed for 2 % in 50 years. But, in Fig. 15a one can observe that greater base shear is observed for medium soil than the firm soil at lower heights of water. This can be explained as follows: due to the effect of SSI, flexibility of the structure varies with soil condition leading to period elongation with the increase in softness of the soil. The ground motions in the periods corresponding to medium soil at lower water levels have high energy content. But as the water level increases, the periods shift leading to higher energy content in ground motions at the periods of the firm soil. The displacement demands are lowest for the firm soil and highest for the soft soil as higher flexibility at the base leads to lower base shear (resistance) and higher drift (see Fig. 16). This response is found to increase with the increase in the hazard level of ground motions and height of water.

Nonlinear-base case For nonlinear base condition, *FootingCondition* 5 is used. Nonlinear Winkler springs are

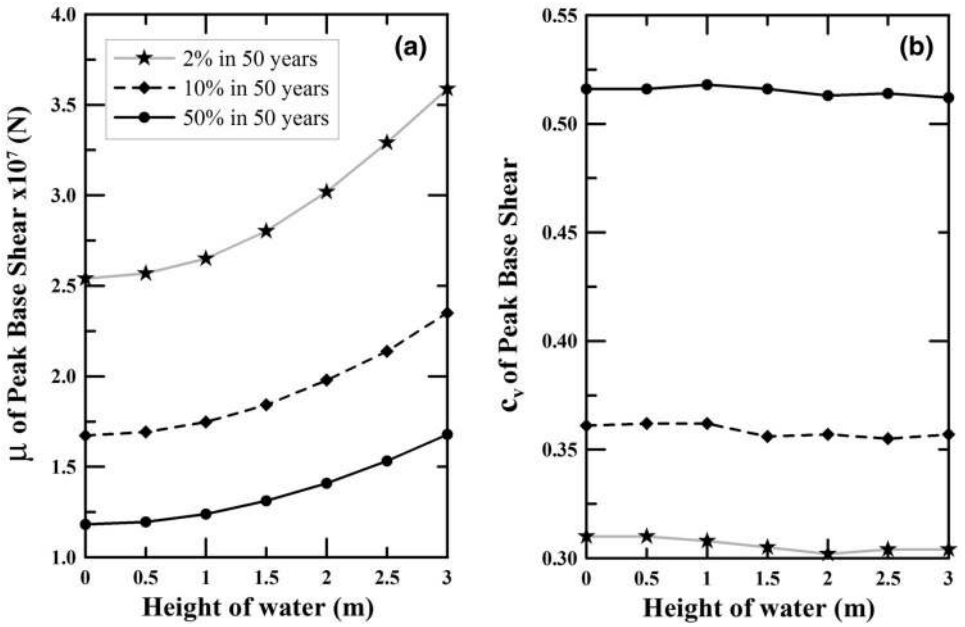

Fig. 14 Peak base shear values for fixed-base case: **a** mean (μ) and **b** coefficient of variation (c_v) for different heights of water, H

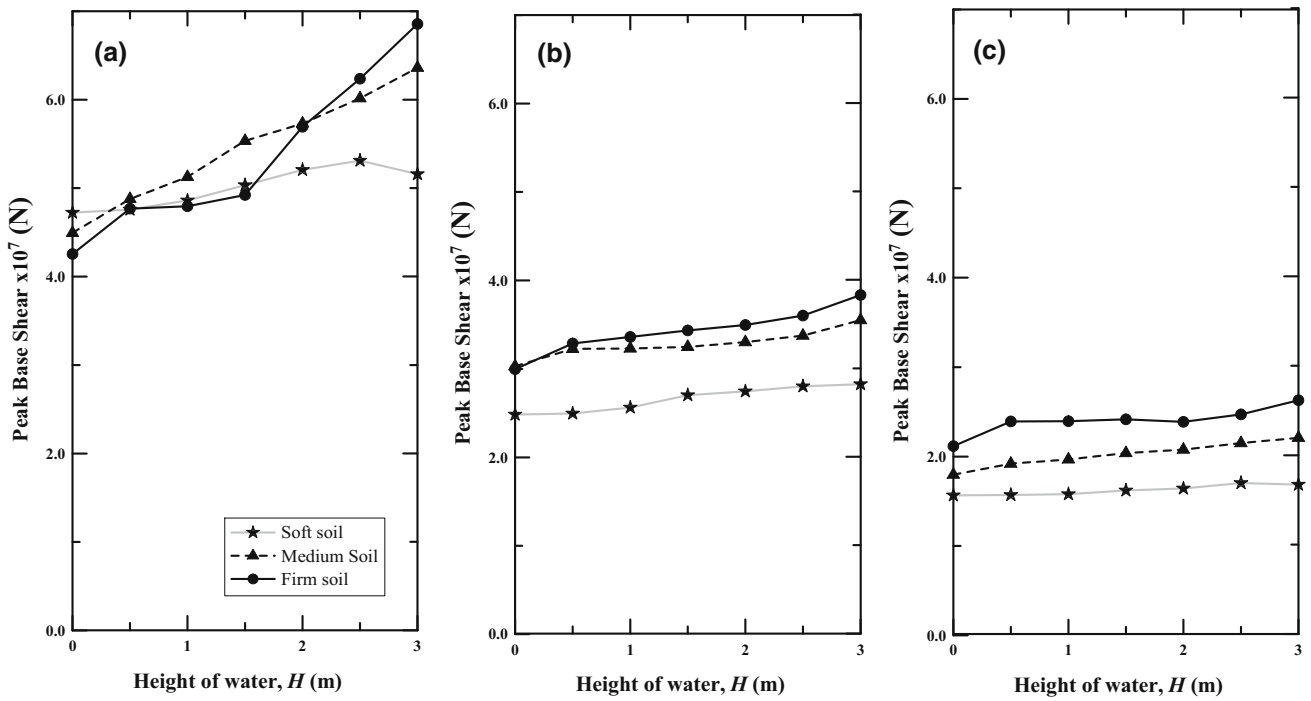

Fig. 15 Mean peak base shear values for (linear) flexible base case at hazard levels: **a** 2 % in 50 years, **b** 10 % in 50 years, and **c** 50 % in 50 years

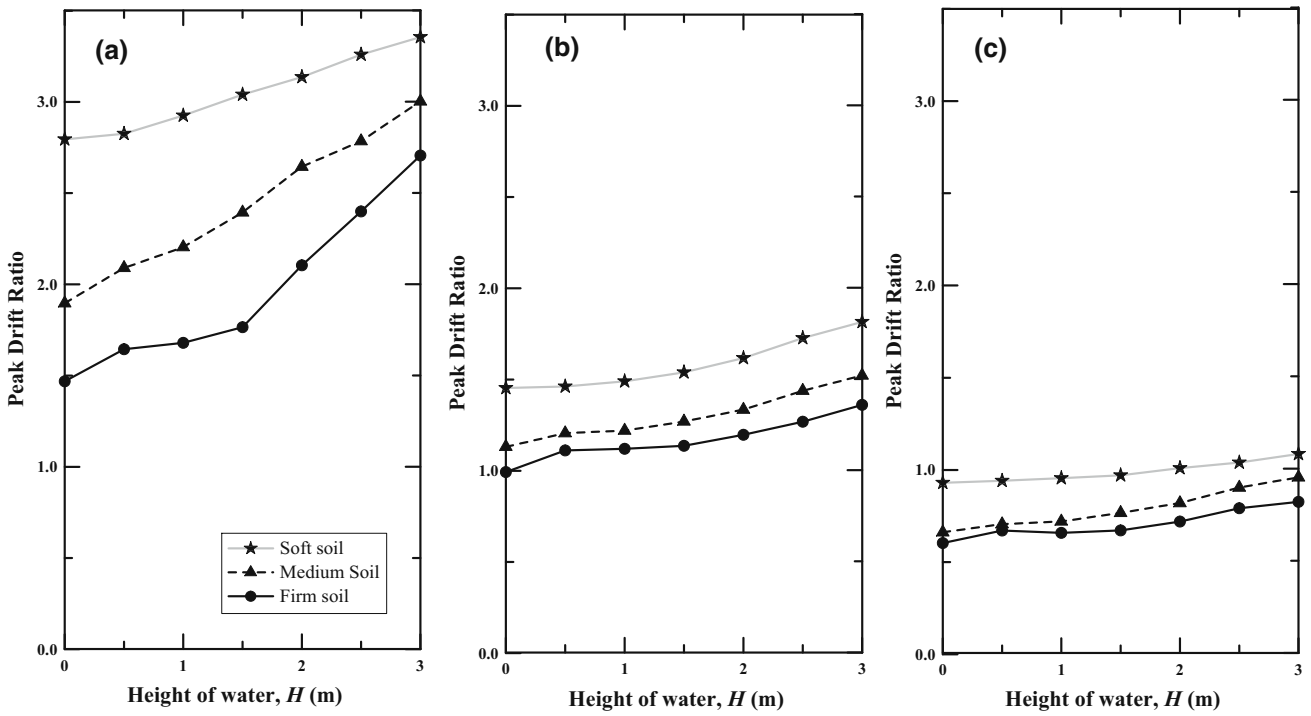

Fig. 16 Mean peak drift ratio values for (linear) flexible base case at hazard levels: **a** 2 % in 50 years, **b** 10 % in 50 years, and **c** 50 % in 50 years

used in the BNWF model representing the soil-foundation system. Mean base shear, mean percentage drift ratio and displacement of the primary structure are recorded in similar fashion to linear base case. Figure 17 show mean peak base shear for different hazard levels, with structure on different soil conditions for nonlinear base case. The

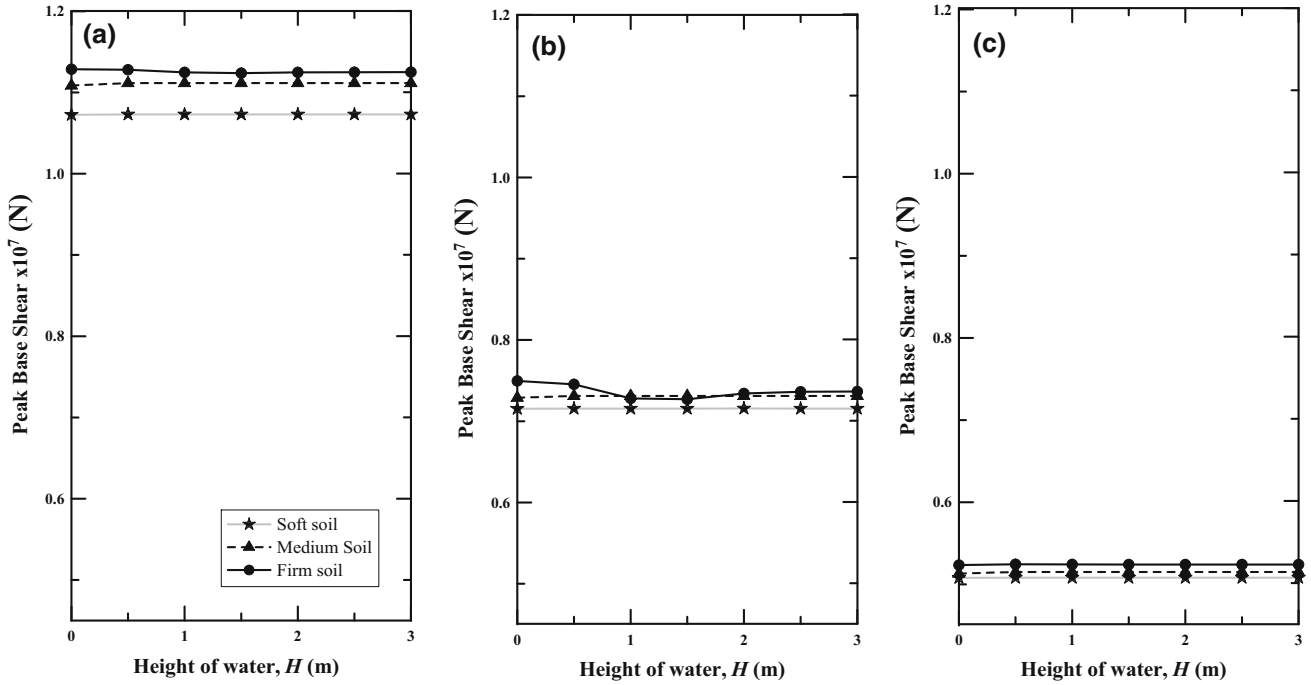

Fig. 17 Mean peak base shear values for (nonlinear) flexible base case at hazard levels: **a** 2 % in 50 years, **b** 10 % in 50 years, and **c** 50 % in 50 years

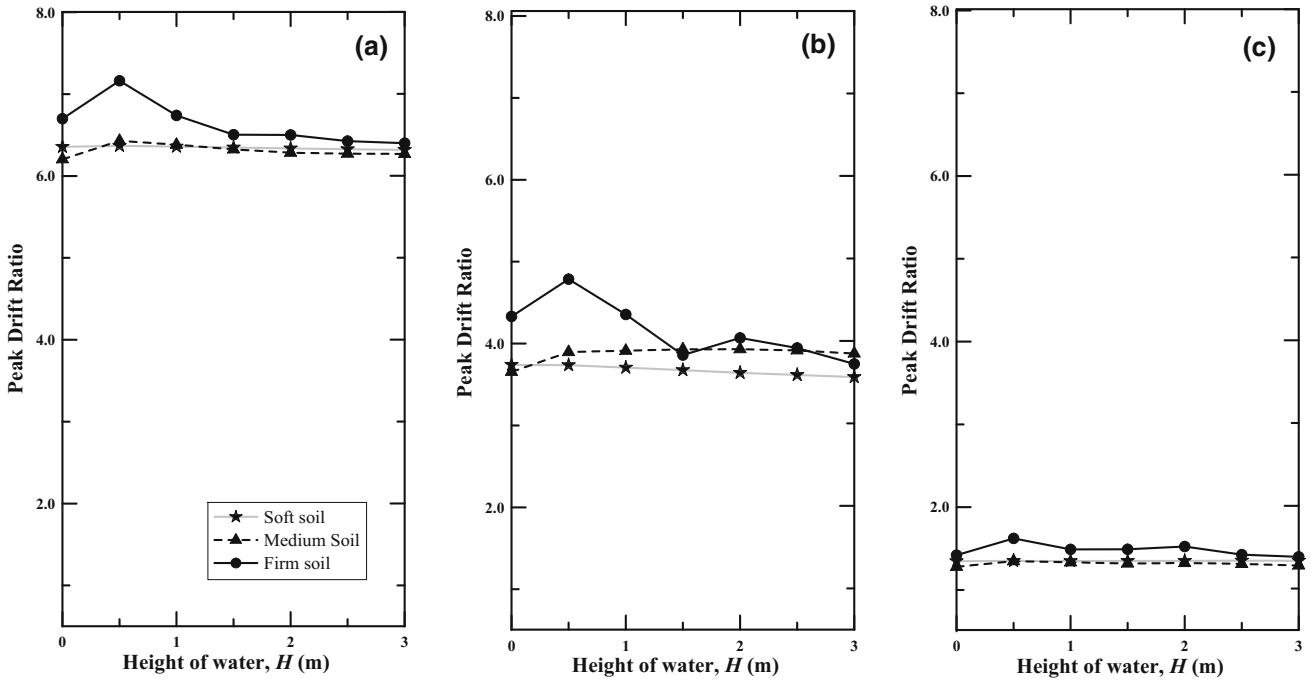

Fig. 18 Mean peak drift ratio values for (nonlinear) flexible base case at hazard levels: **a** 2 % in 50 years, **b** 10 % in 50 years, and **c** 50 % in 50 years

force demands do not increase significantly with increase in height of water as in linear base case (Fig. 17). This is due to the fact that, when the nonlinear Winkler springs reach nonlinear zone (plastic behavior) due to stronger ground motions, their resistance reaches maximum. Similar to linear base case, soft soil shows the lowest base shear,

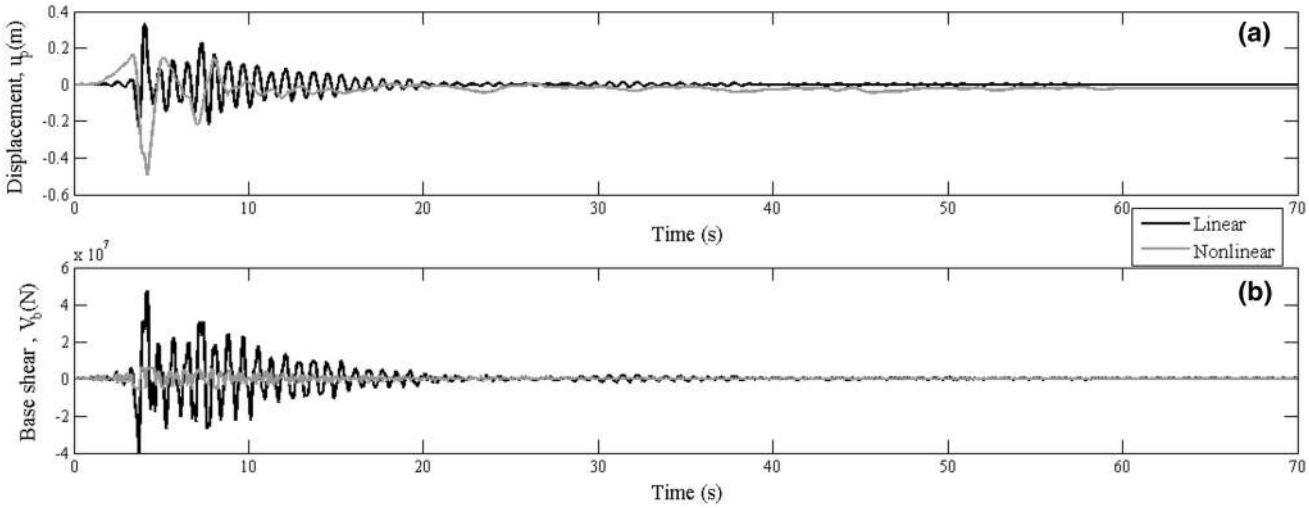

Fig. 19 Time histories of displacement, u_p and base shear V_b for LA-28 with water height of 1.5 m

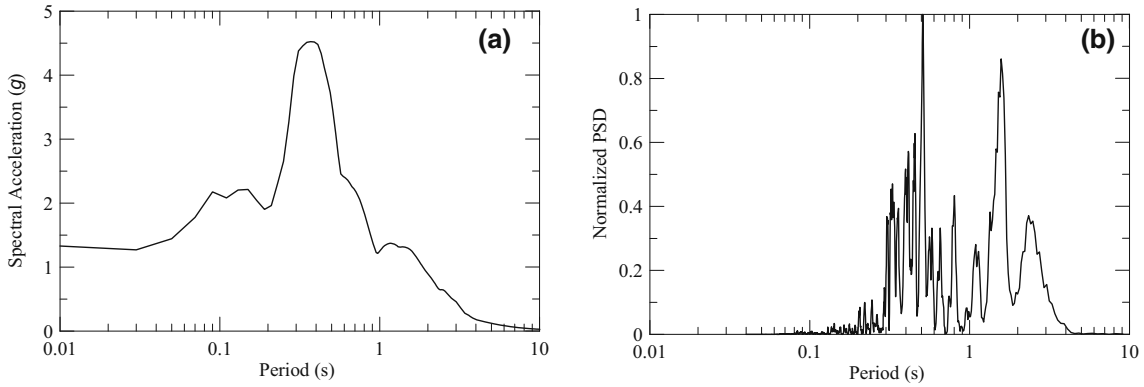

Fig. 20 Characteristics of LA-28 motion: **a** acceleration response spectrum and **b** normalized power spectral density

while firm soil provides the highest base shear. But the trend of drift ratio deviates from that of the linear base case (Fig. 18). This is because of the nonlinear behavior of the soil-foundation interface.

Comparison of linear and nonlinear base cases

Figure 19 shows the comparison of time histories for displacement and base shear demands of linear and nonlinear base cases for LA-28. Figure 20 shows the acceleration response spectrum and normalized power spectral density of LA-28. It can be observed from these figures that this motion contains significant energy around the fundamental period of flexible base aqueduct structure. From Fig. 19, the displacements are observed to be very high for the nonlinear base case when compared to the linear base case. This is because the energy is dissipated in the nonlinear base case leading to the increased period, displacements and a reduced resistance at the base. A permanent deformation is observed in the displacement time history of nonlinear case. Figure 21 shows the ratio of base shear in nonlinear case to the linear case for different hazard levels and soil conditions. These ratios are found to be less than unity in all the hazard level cases. Similarly, Fig. 22 shows the ratios of drift for nonlinear case to the linear one. All hazard level cases show these ratios greater than unity corroborating the aforementioned explanation. From Figs. 21 and 22, the ratios of both base shear and drift ratio decrease with the increase in height of water. One can thus state that the significance of soil nonlinearity decreases for drift ratio and increases for base shear with an increase in height of water, the highest effect being on firmer soils in both base shear and drift ratio.

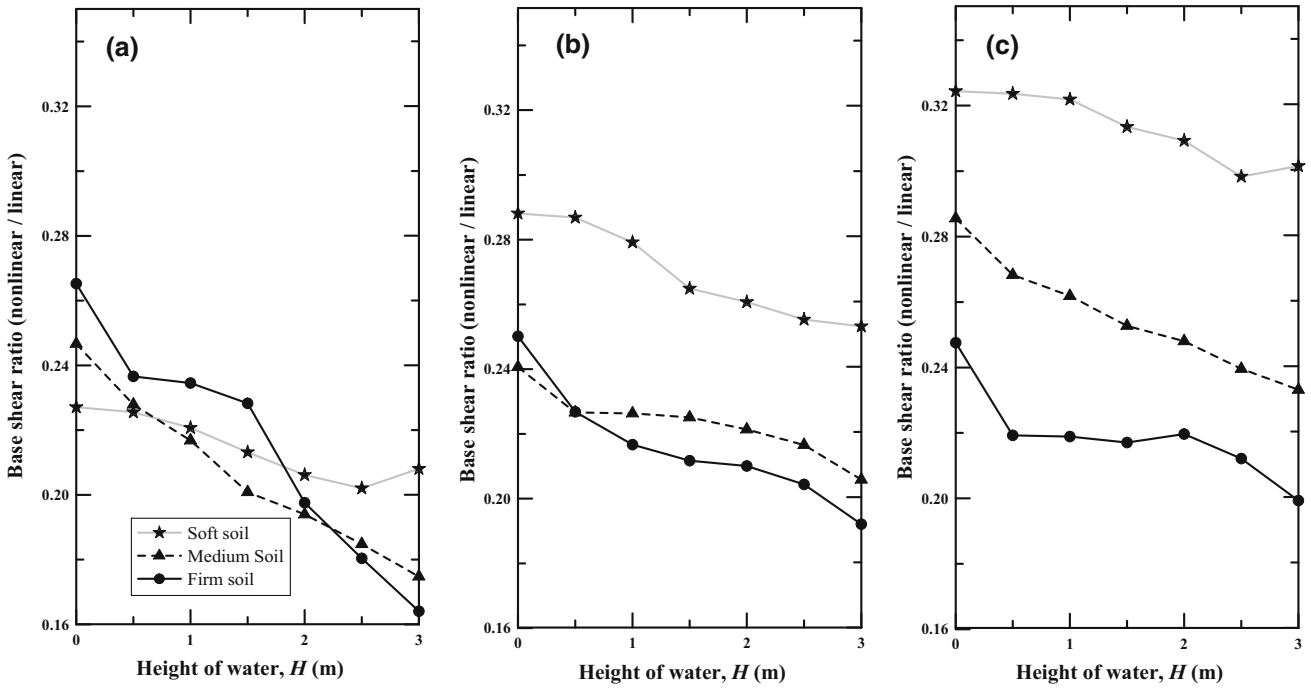

Fig. 21 Ratio (nonlinear to linear) of peak base shear for hazard levels: **a** 2 % in 50 years, **b** 10 % in 50 years and **c** 50 % in 50 years at different water heights

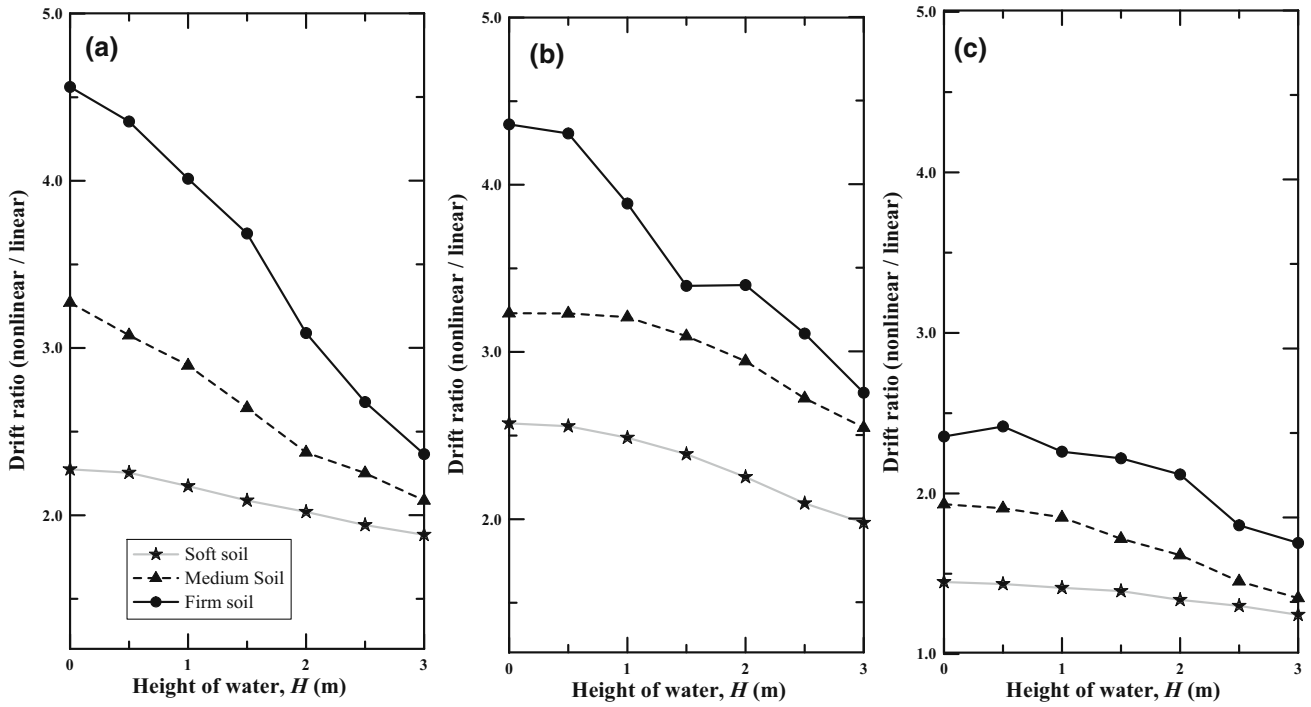

Fig. 22 Ratio (nonlinear to linear) of peak drift ratios for hazard levels: **a** 2 % in 50 years, **b** 10 % in 50 years and **c** 50 % in 50 years at different water heights

Conclusions

In this study, a representative model of an elevated aqueduct is considered with different base fixity conditions. Frequency domain as well as time domain analysis have been performed and demand parameters such as base shear and drift ratio are studied for varying heights of water in channels and different soil conditions at the site. Some of the important findings of this study are as follows:

1. The period of the aqueduct structure increases drastically from 0.025 s in fixed base case to 0.52, 0.59 and 0.743 s for firm, medium and soft soil conditions, respectively. This increase in period from the fixed to the flexible base case can be explained by considering the relative stiffness of the structure (which is very high due to long shear wall) in comparison to the foundation springs. Thus, to capture the dynamic behavior reasonably, it is important to model the base fixity appropriately.
2. With increase in height of water in channels, only a nominal increase in the natural period of the structure is observed. Further, the periods of convective masses, which are high enough compared to the period of the structure, are not affected significantly due to change in base conditions.
3. In case of fixed-base analysis, the RMS values of response for different water depths are observed to follow the same trend as that of the amplitude of its transfer function at the natural frequencies of the convective water masses. This indicates high influence of the convective mass on the response of the structure for frequency domain analysis. This influence of the convective mass is not however observed for the time history analysis of the fixed base case. This is because in time history analysis, the ground motions do not have significant energy to excite the convective modes.
4. For frequency domain analysis of elastic base case, the base shear demand is found to be higher for firmer soil conditions. Further, response increases with the increase in height of water and decrease in soil flexibility. A similar trend is also observed from the time history analysis.
5. Introduction of nonlinearity at soil-foundation interface leads to increase in drift ratio and decrease in base shear compared to the linear base case. Negligible effect on the response due to change in the height of water is found for the nonlinear case due to mobilization of soil at the base.
6. The decrease in base shear is higher in firmer soils from linear to nonlinear base case for ground motions with 50 % in 50 years hazard level. This trend is however not significant for ground motions with 2 % in 50 years hazard levels due significant nonlinearity at the soil-foundation interface for such a high hazard level.
7. From time history analysis, it is observed that for all hazard levels, base shear is lower for the nonlinear base case than the elastic base case. The trend is opposite for drift ratio, i.e., drift ratio is higher for nonlinear base case in comparison to the linear base case. Also, this ratio of nonlinear to linear responses (of base shear and drift) reduces with an increase in height of water in the channels. This is because, for varying water levels, these responses are least affected in nonlinear base case and get altered only in case of elastic base. In general, for a given hazard level (say 10 % in 50 years), the base shear demand of empty aqueduct is maximum for elastic base case, followed by fixed base and nonlinear base cases.

The results of this study are limited to the parameter space considered, ground motions and PSDFs used, and modeling assumptions. Further, this study does not consider the hydrodynamic effects that may be present in case the piers are submerged in water. The findings of this study may however provide a better understanding of seismic behavior of an elevated aqueduct under various modeling assumptions and input excitations.

References

Boulanger R, Curras C, Kutter B, Wilson D, Abghari A (1999) Seismic soil-pile-structure interaction experiments and analyses. ASCE J Geotech Geoenvironmental Eng 125(9):750–759

Bowles J (1988) Foundation analysis and design. McGraw-Hill Publishing Company, USA

Dey A, Gupta VK (1999) Stochastic seismic response of multiply-supported secondary systems in flexible-base structures. Earthq Eng Struct Dynam 28(4):351–369

Gazetas G (1991a) Formulas and charts for impedances of surface and embedded foundations. ASCE J Geotech Eng 117(9):1363–1381

Gazetas G (1991b) Foundation vibrations. In: Foundation Engineering Handbook. Springer

Gutierrez JA, Chopra AK (1978) Evaluation of methods for earthquake analysis of soil-structure interaction. In: Proceedings of the Sixth World Conference on Earthquake Engineering, vol 6. Berkely

Harden C, Hutchinson T, Martin GR, Kutter BL (2005) Numerical modeling of the nonlinear cyclic response of shallow foundations. In: Tech. rep., Pacific Earthquake Engineering Research Center, College of Engineering. University of California, Berkeley

Housner GW (1954) Earthquake pressures on fluid containers. Tech. rep. California Institute of Technology, Pasadena

Idelsohn S, Onate E, Del Pin F, Calvo N (2006) Fluid-structure interaction using the particle finite element method. Comput Methods Appl Mech Eng 195:2100–2123

Kiureghian AD, Neuenhofer A (1992) Response spectrum method for multi-support seismic excitations. Earthq Eng Struct Dynam 21(8):713–740

Liu WK (1981) Finite element procedures for fluid-structure interactions and application to liquid storage tanks. Nucl Eng Des 65(2):221–238

OpenSees (2012) Open system for earthquake engineering simulation: OpenSees. Pacific Earthquake Engineering Research Center (PEER), Richmond

Ramaswamy B, Kawahara M (1987) Arbitrary Lagrangian-Eulerianc finite element method for unsteady, convective, incompressible viscous free surface fluid flow. Int J Numer Meth Fluids 7(10):1053–1075

Ray Chaudhuri S, Gupta VK (2003) Mode acceleration approach for generation of floor spectra including soil-structure interaction. Int J Earthq Technol 40:99–115

Raychowdhury P (2011) Seismic response of low-rise steel moment-resisting frame (SMRF) buildings incorporating nonlinear soil-structure interaction (SSI). Eng Struct 33:958–967

Raychowdhury P, Hutchinson TC (2009) Performance evaluation of a nonlinear winkler-based shallow foundation model using centrifuge test results. Earthq Eng Struct Dynam 38:679–698

Raychowdhury P, Singh P (2012) Effect of nonlinear soil-structure interaction on seismic response of low-rise SMRF buildings. Earthq Eng Eng Vib 11(4):541–551

Raychowdhury P, Hutchinson TC (2008) ShallowFoundationGen Opensees Documentation

Valeti B (2013) Seismic analysis of a river aqueduct considering soil-structure interaction and hydrodynamic effects. Master's thesis, Indian Institute of Technology Kanpur, Kanpur, UP, 208016, India

Villaverde R (2009) Fundamental Concepts of Earthquake Engineering. Taylor and Francis Group, UK

Westergaard H (1933) Water pressures on dams during earthquakes. Trans Am Soc Civ Eng 98(2):418–433

Wong HL, Luco JE (1985) Tables of impedance functions for square foundations on layered media. J Soil Dyn Earthq Eng 4(2):64–81